Density functional study of $PbTiO_3$ nanocapacitors with Pt and Au electrodes

W. A. Al-Saidi and Andrew M. Rappe
The Makineni Theoretical Laboratories, Department of Chemistry, University of Pennsylvania, Philadelphia, Pennsylvania 19104-6323, USA

(Received 29 May 2010; revised manuscript received 8 September 2010; published 4 October 2010)

We present an *ab initio* density functional study of ferroelectricity in single-domain $PbTiO_3$-based nanocapacitors. We used density functional theory with the recently introduced PBEsol generalized-gradient exchange-correlation functional, which we found to give accurate properties of bulk ferroelectric (FE) materials. Pt and Au electrodes are used in our study to gain a thorough understanding of the electrode-oxide interfaces, and the role of the interfacial chemical bonding and charge transfer in stabilizing the FE polar phase. We found that the FE properties of the thin films depend not only on the electrode and the FE material but also on the electrode-perovskite termination (TiO_2 vs PbO), exemplifying the key role of the interface in these systems. The critical thickness was found to be 24–28 Å. In addition, a Löwdin orbital analysis gives a detailed description of the distribution of charges in the system, and shows the importance of charge passivation by the electrodes in stabilizing the FE polar phase.

DOI: 10.1103/PhysRevB.82.155304 PACS number(s): 82.65.+r, 68.35.Md

I. INTRODUCTION

Ferroelectric (FE) nanocapacitors have attracted a lot of attention in the past few years, due to their potential use for nonvolatile FE random access memory devices. Recently, memory density of up to a terabit per square inch has been obtained[1,2] in FE nanocapacitors based on $BaTiO_3$ (BTO) and lead zirconate titanate. An issue of particular importance for microelectronic applications is how thin the FE film can be made before it loses its FE property.

Ferroelectricity is a collective phenomenon triggered by a condensation of "soft phonon mode;" in the perovskites, this involves the displacements of the cations from their oxygen cages coupled to a lattice distortion. In a thin-film geometry, the accumulated charges at the interface, if left uncompensated, would lead to a depolarizing field which suppresses the FE behavior of thin films.[3] Thicker ferroelectric films in short-circuited nanocapacitors will have weaker depolarizing fields, proportional to the inverse of the film thickness. The critical thickness for ferroelectricity in nanocapacitors has been investigated using different approaches previously. One of the first studies where the electrodes are treated from first principles was done by Junquera and Ghosez,[4] and was followed afterward by several other studies.[5–12] Stengel *et al.* introduced a method to determine the critical thickness in nanocapacitors which is based on the generalized capacitance calculated using a finite-field approach.[13]

In this paper, we use an *ab initio* density functional theory (DFT) approach including the recently introduced PBEsol functional[14] to investigate the properties of several $PbTiO_3$ (PTO)-based nanocapacitorlike structures. In principle, DFT is an exact theory, as defined by a universal exchange-correlation energy functional, but in practice, it resorts to an approximate form of the functional within the Kohn-Sham formalism. The local-density approximation (LDA) (Ref. 15) of the exchange-correlation functional is well known to underestimate the experimental lattice constants by 1–2 %, which is generally an acceptable error. However, in FEs this poses a serious problem because the FE instability is extremely sensitive to volume changes. Typically, in the FE community, this problem is partially remedied by using the experimental lattice constant; obviously this remedy can only be used for experimentally studied materials. The generalized-gradient-approximation (GGA) functional of Perdew, Burke, and Ernzerhof (PBE),[16] which generally constitutes a significant improvement over LDA, often exaggerates the FE properties, such as those of PTO and BTO. Recently, Wu and Cohen (WC) introduced a new functional based on the GGA-PBE functional; WC gives accurate values of the FE properties.[17]

In the study of FE nanocapacitors, most groups have used LDA,[4,5,10,13,18] and to a lesser extent the GGA-PBE functional.[6,8,9,11] Umeno *et al.*[7] examined FE thin films with LDA and GGA-PBE functionals, and showed that GGA-PBE gives stronger FE properties than the LDA functional. In the present study we used PBEsol,[14] which belongs to the GGA family. In this functional, the first-principles gradient expansion for the exchange is restored over a wide range of density gradients. This makes PBEsol more accurate for solids and surfaces, as was shown by Perdew and collaborators,[16] while the PBE functional[16] is better suited for atoms and molecules. As far as we know, this study is one of the first applications of PBEsol to FE materials.

II. METHODOLOGY

In our DFT calculations, we used modified versions of ABINIT (Ref. 19) and PWSCF.[20] Core electrons are replaced by norm-conserving pseudopotentials,[21] which are generated using OPIUM.[22] For Ti, we included the semicore electrons $3s^2$ and $3p^6$ due to the large overlap with the valence states.[23] For Pb, we included the $5d^{10}$ electrons in the valence sector. We used a plane-wave cutoff of 25 hartree, which was sufficient to ensure a convergence of ≈ 1 mhartree on total energies. The reciprocal-space integration was performed using a $4\times4\times1$ Monkhorst-Pack[24] k-point mesh which we found to be sufficient.

TABLE I. Lattice constants in angstrom of the cubic phases of STO, PTO, and BTO perovskites, and fcc Pt and Au metals obtained using different density functionals.

	LDA	PBE	WC	PBEsol	Expt.
STO	3.863	3.947	3.906	3.907	3.905[a]
PTO	3.894	3.976	3.934	3.934	3.93[b]
BTO	3.964	4.034	3.991	3.991	4.00[c]
Pt	3.905	3.941	3.919	3.910	3.92[d]
Au	4.046	4.125	4.077	4.063	4.08[d]

[a]Reference 25.
[b]Reference 26.
[c]Reference 27.
[d]Reference 28.

We used a supercell approach to represent the capacitor-like FE thin film. The supercell contains an alternating stack of PbO and TiO_2 layers, sandwiched between metal electrodes with (100) orientation. The periodic boundary conditions of the supercell geometry impose a short-circuit condition between the electrodes.[8] We considered both TiO_2 and PbO interfaces with the metal electrodes. In the case of the TiO_2 termination and with an electrode M, the supercells have the general formula $(M_2)_m/TiO_2$-$(PbO\text{-}TiO_2)_n/(M_2)_{m+1}$, and in the case of the PbO termination the formula is $(M_2)_m/PbO$-$(TiO_2\text{-}PbO)_n/(M_2)_{m+1}$. Here $(2m+1)$ is the number of the electrode layers and n is the number of $PbTiO_3$ unit cells. We investigated values of $n=1,\ldots,11$. Also, we examined different electrode thicknesses $m=4,\ldots,7$ layers, and found that 4–5 layers are sufficient. The registry for the metal atoms is on top of the oxygen atoms for the TiO_2 termination, and on top of the A cation and oxygen atom for the PbO termination.

FE properties are very sensitive to the in-plane lattice constant, and this, in addition to the DFT functional used, mostly explains the wide spread values of the critical thickness of FE thin films in *ab initio* studies.[4,6,7] Typically, the capacitor hetrostructure is grown epitaxially on a thick $SrTiO_3$ (STO) substrate; the in-plane lattice constant of the FE materials and the electrodes are thus constrained by the bulk STO lattice constant. In our calculations, we used the experimental lattice constant (3.905 Å) of STO. The GGA-PBEsol functional yields a value which is in excellent agreement with this value (see Table I). The initial geometry is built from the primitive bulk unit cell either in the paraelectric (PE) or the FE phase. The final optimized structure is obtained by relaxing the strain and all of the atomic coordinates along the (100) direction until the forces are less than 5 meV/Å.

III. RESULTS AND DISCUSSION

A. Bulk properties with GGA-PBEsol

The first task is to establish the validity of the GGA-PBEsol functional for the study of the bulk systems we are interested in. To this end we studied the perovskites STO, PTO, and BTO in their cubic phases, as well as face-centered-cubic (fcc) structures of the metals Pt and Au. Table I summarizes the properties of the optimized structures computed using LDA, GGA-PBE, and GGA-WC functionals in addition to the GGA-PBEsol functional. In all of these systems, GGA-PBEsol gives results that are comparable or in better agreement with the experimental values than the other functionals.

Next, we investigated bulk PTO and BTO in the tetragonal FE phase. Table II summarizes our results using different functionals. It is gratifying that GGA-PBEsol yields FE properties in good agreement with the experimental values. The optimized geometries obtained with GGA-PBEsol are in better agreement with experimental values than both the LDA and GGA-PBE values, and are very comparable to those obtained using the GGA-WC functional. This also holds for the cation rumplings and the polarization computed using the modern theory of polarization.[31]

What is particularly interesting in the results of Tables I and II is that the results obtained with the GGA-WC and GGA-PBEsol functionals are very close, despite the different exchange-enhancement forms these functionals use. We have also examined some of our nanocapacitors using the WC functional and found close resemblance in the results. This is

TABLE II. Fully relaxed bulk FE properties of tetragonal PTO and BTO obtained using LDA, GGA-PBE, GGA-WC, and GGA-PBEsol functionals. a is the in-plane lattice constant and c/a is the tetragonality. δ_{Ti}, δ_{Pb}, and δ_{Ba} are the rumplings of the cations from their oxygen cages. P (C/m^2) is the polarization obtained using the Berry phase approach. All distances are in angstrom.

	$PbTiO_3$					$BaTiO_3$				
	a	c/a	δ_{Pb}	δ_{Ti}	P	a	c/a	δ_{Ba}	δ_{Ti}	P
LDA	3.86	1.05	0.39	0.30	0.85	3.965	1.006	0.06	0.08	0.21
GGA-PBE	3.85	1.25	0.96	0.53	0.89	4.000	1.047	0.20	0.19	0.46
GGA-WC	3.88	1.10	0.54	0.38	0.96	3.975	1.023	0.12	0.14	0.41
GGA-PBEsol	3.875	1.10	0.51	0.38	1.00	3.976	1.023	0.12	0.14	0.41
Expt.	3.88[a]	1.071[a]			0.5–1[b]	3.986[c]	1.010[c]			0.27[d]

[a]Reference 26.
[b]Reference 29.
[c]Reference 27.
[d]Reference 30.

TABLE III. Computed properties of PTO-based nanocapacitors with different electrodes. N_c is the smallest number of unit cells for which the film has a FE ground state. The layer polarization at the negative (P_-) and positive (P_+) interfaces, and the average polarization (P_{av}) of the FE film, are all in units of the bulk polarization P_{bulk}. c/c_{bulk} measures the tetragonality of the FE film in units of the bulk value, and Δ (meV) is the well depth of the FE film per surface unit cell.

	N_c	P_-/P_{bulk}	P_+/P_{bulk}	P_{av}/P_{bulk}	c/c_{bulk}	Δ
TiO_2 term						
Pt/PTO/Pt	7	0.50	0.62	0.62	0.94	7
Au/PTO/Au	7	0.77	0.86	0.80	0.96	16
PbO term						
Pt/PTO/Pt	6	0.99	0.97	0.95	0.96	45
Au/PTO/Au	6	0.44	0.38	0.35	0.96	31

also true for the work functions of Pt and Au metals.

Finally, we note that our results obtained with the LDA, GGA-PBE, and GGA-WC functionals are in very good agreement with previous calculations; see, for example, Refs. 17 and 32.

B. Critical thickness of ferroelectricity

As discussed in Sec. I, the critical thickness is determined by the competition between the electrostatic energy associated with the depolarizing field and the energy gain due to the FE ordering. In order to determine the critical thickness of the nanocapacitors, we started the oxide layers with either a bulk FE or PE structure, relaxed the coordinates, and compared the energies. For this study, we focused on systems with an odd number of oxide layers and equally thick top and bottom electrodes so that the entire film can access a state with perfect up-down mirror symmetry (when all rumplings are zero).

We find that only capacitors with a thickness >24–28 Å can sustain a FE instability. Table III gives a summary of these capacitors. For the TiO_2 termination, the critical thickness is seven unit cells ≈28 Å with either Pt or Au electrodes. For the PbO termination, the critical thickness is six unit cells. Table III also shows the interfacial polarization at the positive and negative surfaces, as well as the average polarization of the FE thin films. The layer polarization, given in units of the bulk polarization, is defined as the ratio of the rumplings of the cations from their oxygen cages in the thin film to those in the bulk. Also, the bulk polarization is determined using an in-plane lattice constant of 3.905 Å and not that of the free sample (3.88 Å), in order to have a fair comparison with the thin films where the in-plane lattice constant was fixed at 3.905 Å.

Our results indicate that the critical thickness of ferroelectricity depends not only on the FE material and the electrodes but also on the termination of the film (TiO_2 vs PbO). For example, with the Pt electrodes, the layer polarization at the positive and negative surfaces is almost half the bulk value with the TiO_2 termination while they attain their bulk value for the PbO termination. This is an indication of the importance of the FE-electrode interface in these nanocapacitors. Also, note that with the TiO_2 termination, the average polarization of the FE thin film with the Pt electrodes is larger than that with the Au electrodes while for the PbO termination, we have the opposite behavior.

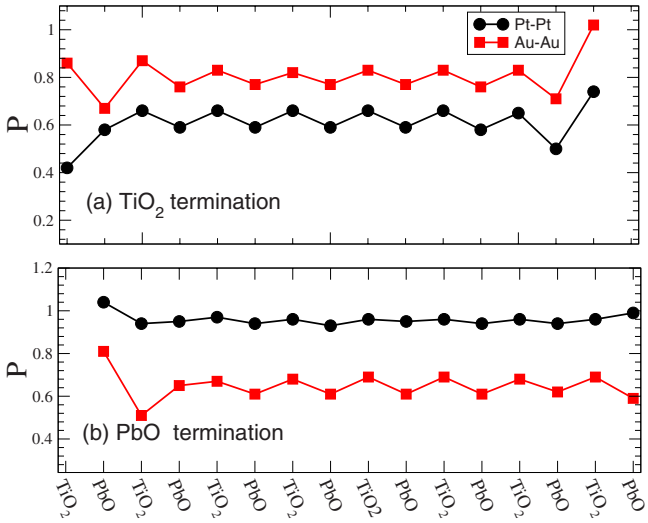

FIG. 1. (Color online) The layer polarization profile for the TiO_2 and PbO nanocapacitors with Pt and Au electrodes. We measure the polarization with respect to the bulk polarization of PTO. All films have seven unit cells.

The average polarization P of the nanocapacitors shown in Table III can be used to estimate the effective screening length λ of the metallic electrodes. Using the electrostatic boundary conditions, we can express the depolarizing polarization in the film as,

$$E_d = -\frac{2\lambda P}{\epsilon_0 \ell}, \tag{1}$$

where ℓ is the thickness of the FE film.[3] We can use our first-principles results to estimate λ after using the macroscopic averaging[33] of the electrostatic potential to calculate the depolarizing field, E_d. We obtain λ=0.045 and 0.028 Å for Pt and Au with TiO_2 termination, and 0.007 and 0.034 Å with PbO termination, respectively. Note that the effective screening length is not a characteristic of the metal but rather it depends on the electrode/thin-film interface. Gerra *et al.* found a value of λ≈0.1 Å for $SrRuO_3/BTO/SrRuO_3$ nanocapacitor.[10] The computed first-principles effective screening length computed using Eq. (1) seems to be much smaller than the accepted screening lengths of metals. (For $SrRuO_3$ it is ≈4 Å, for Pt it is ≈0.5 Å, and for Au it is ≈0.8 Å.)

C. Structural properties of the nanocapacitors

Figure 1 gives a detailed view of the layer polarization of all of the oxide layers for both the TiO_2 and PbO terminations with Pt and Au electrodes. In these calculations, we used a thin film with 15 oxide layers. From the figure, we can see that in all of the cases the layer polarization shows an

TABLE IV. Bucklings (in Å) of the electrode layers that are in registry with the PbO layers. We report these values for the PE nanocapacitors (β_0), and for the negative (β_-) and positive (β_+) surfaces of the FE nanocapacitors.

	PbO termination			TiO_2 termination		
	β_0	β_-	β_+	β_0	β_-	β_+
PtPt						
First	−0.347	−0.314	−0.023	0.012	0.007	0.017
Second	0.019	0.013	0.021	−0.005	0.008	−0.015
Third	0.000	−0.011				
AuAu						
First	−0.195	−0.247	0.074	−0.062	−0.015	0.068
Second	−0.041	−0.064	0.006	−0.013	−0.008	−0.005
Third	−0.000	−0.043				

anomalous behavior at the oxide-electrode interface, where the layer polarization is either enhanced or diminished compared to the polarization in the layers far from the electrode. The effects of the interface extend for only 1–2 layers, and then the layer polarization becomes homogeneous. Away from external perturbations, a uniform polarization is energetically favorable, as can be seen from a Landau-Ginzburg-Devonshire point of view.

Table IV shows the buckling in the electrode layers that are in registry with the PbO layer for the PE nanocapacitors (β_0), and for the negative (β_-) and positive (β_+) surfaces of the FE nanocapacitors. A negative value of the buckling indicates that the metal atom that is in registry with the oxygen atom is closer to the oxide than that on top of the *A* cation. There is no buckling in the electrode layers that are in registry with the TiO_2 layers because the two metal atoms have symmetrical chemical environments.

The results for the electrode layer bucklings show similar behavior to what has been seen before with the rumplings in the oxide layers. The interfacial electrode layers have the largest bucklings, and the buckling amplitude decays for layers deeper in the electrode. For example, with Pt electrodes, the buckling in the first Pt layer attached to the PE film is −0.347 Å, and decays to 0.019 Å in the next buckled layer (third Pt layer) which is ≈6 Å from the interface. Also, note that β_0 and β_- are very close to each other since the polarization of the film and the intrinsic interfacial dipole are parallel to each other. At the positive surface, the interfacial dipole and the FE polarization oppose each other and thus greatly reduce the bucklings in the electrode layers.

The size of the bucklings of the Pt and Au electrode layers correlates well with the strength of the interfacial bonding between the metal and oxide layers, which is larger for Pt-O than it is for Au-O. This can be seen, for example, from the bond enthalpy, which is 347 kj/mole for Pt-O and 222 lj/mole for Au-O.

D. Electronic properties of nanocapacitors

To gain further insight into the electronic structure of the nanocapacitors, we have performed a Löwdin orbital analysis[34] and a layer-projected density of states (LPDOS) on the optimized structures. We compare and contrast the PE and FE nanocapacitors with Pt and Au electrodes, as well as with both TiO_2 and PbO terminations.

TABLE V. Electronic charge gain/loss (relative to bulk atoms) for atoms in the first and second interfacial layers determined using a Löwdin orbital analysis. Both the TiO_2 and PbO terminations are considered. We show the charge transfer for the PE nanocapacitor (ρ_0) as well as the values for the negative (ρ_-) and positive (ρ_+) surfaces of the FE nanocapacitor, respectively. For each electrode and termination, we show also the total charge gain/loss in the first and second interfacial layers. Charge transfer is measured in millielectrons. All the thin films have 15 oxide layers (seven unit cells).

TiO_2 termination							
	ρ_0	ρ_-	ρ_+		ρ_0	ρ_-	ρ_+
Pt	247	316	172	Ti	80	70	45
Pt	247	316	172	O	−254	−239	−256
Pt	30	24	33	Pb	−35	−20	−31
Pt	45	45	40	O	−21	−22	−14
Tot	569	701	417	Tot	−484	−450	−512
Au	173	313	87	Ti	11	−41	19
Au	173	313	87	O	−142	−143	−160
Au	3	1	9	Pb	−12	−15	−25
Au	5	7	9	O	−46	−18	−33
Tot	354	634	192	Tot	−331	−360	−359
PbO termination							
Pt	306	348	270	Pb	−217	−165	−293
Pt	104	139	8	O	−262	−109	−283
Pt	28	19	29	Ti	24	−4	9
Pt	28	19	29	O	−22	−4	−14
Tot	466	525	336	Tot	−499	−286	−595
Au	242	293	36	Pb	−200	−158	−267
Au	76	115	220	O	−188	−134	−179
Au	5	7	11	Ti	17	3	5
Au	5	7	11	O	−14	−2	−22
Tot	328	422	278	Tot	−399	−293	−485

Löwdin orbital analysis, which is obtained from the projection of the periodic ground-state orbitals onto a localized set of atomic orbitals, has a large degree of arbitrariness and gives only a qualitative view of distribution of charge in the system. In our charge analysis, we focused on the charge rearrangements at the interfaces, especially the differences between the charges of the interfacial atoms and those of the "bulk" atoms that are far from the interface. Table V shows the change in electronic charge for atoms in the first and second interfacial layers for the PE (ρ_0), and the negative (ρ_-) and positive (ρ_+) surfaces of the FE nanocapacitors.

First, we examine the nanocapacitors with the TiO_2 termination. In this case, the two electrode atoms are symmetric because they are in registry with the two oxygen atoms in the TiO_2 layer. In the PE capacitors with Pt electrodes, the first interfacial electrode layer gains 494 millielectrons (milli-*e*).

The second Pt layer, in registry with the PbO layer and farther away from the interface, gains less (75 milli-*e*). For deeper electrode layers, there is almost no charge gain or loss (less than ≈5 milli-*e*). The orbital decomposition of the Löwdin charges reveals that most of the gain in the electrodes is in the *s* and *p* channels, and to a lesser extent in the *d* channel. The oxygen atoms in the TiO_2 layer lose 254 milli-*e*/atom, almost equally from the *s* and *p* channels, in accord with a hybridization with the *s* and *p* orbitals of the metal atoms. Note also that the cations play a relatively smaller role in charge transfer: Ti gains 80 milli-*e* mostly in the *d* channel, and Pb loses 35 milli-*e* mostly from the *s* channel. Overall, the electrode interfacial layers gain 569 milli-*e* while the oxide layers lose 484 milli-*e*. The system is of course charge neutral, and charges lost in one part of the system should appear in another part. However, a discrepancy between the positive and negative charges is to be expected in a Löwdin orbital analysis which does not rigorously satisfy the sum rule (e.g., there could be some delocalized charges that are not captured by a projection of the wave function onto a small set of localized orbitals). The important point of this analysis is the large changes in the Löwdin charges with the FE distortion, as explained below.

In the FE films with either electrode, either termination, and for either polarization, there is a net charge transfer from the oxide to the electrode atoms. However, it is more relevant to consider the additional charge transfers as the PE film becomes FE. In the case of Pt electrode and TiO_2 termination, the negative surface gains charge of 138 milli-*e* (=316+316−247−247) while that on the positive surface loses 150 milli-*e*. Most of the charge-transfer changes in the electrode atoms are in the *d* channel, and to a lesser extent in the *p* channel. Also, in comparison to the PE film, the negative TiO_2 interfacial layer gains 20 milli-*e* (mostly in the oxygen *s* channel), and the positive surface loses 39 milli-*e* (mostly in the Ti *d* channel). There are also some changes in the PbO layer, but they are much smaller, as can be seen from the table. Overall, the Pt electrode gains 701 milli-*e* on the negative surface, and 417 milli-*e* on the positive surface. On the other hand, the oxide layers lose 450 milli-*e* on the negative surface and 512 milli-*e* on the positive surface. On either the negative or the positive surfaces, there seems to be a large discrepancy between the charges which are lost by the oxide layers and those which are gained by the electrodes. However, this discrepancy can be accounted for due to a charge passivation by the electrodes which is taking place in the form of charge transfer between the positive and negative sides of the capacitor, transported by the electrodes.

In the PbO-terminated films, it is clear that Pb plays a more prominent role in charge transfer, compared to that of Ti in the TiO_2-terminated films. In all of the nanocapacitors, both oxygen and Pb in the interfacial PbO layer lose some electronic charge while the electrode atoms gain charge. In the PE film, the orbital decomposition shows that the Pt atoms gain charge. It is rather surprising that the metal atom in registry with Pb gains more charge than that in registry with oxygen. Pb loses charge mostly from the *s* channel, and also to a lesser extent from the *p* and *d* channels. Oxygen also loses charge almost equally from the *s* and *p* channels. In the FE case, and as seen before with the TiO_2 termination, the electrode atoms on the negative surface gain charge and those on the positive surface lose charge in comparison to the PE case.

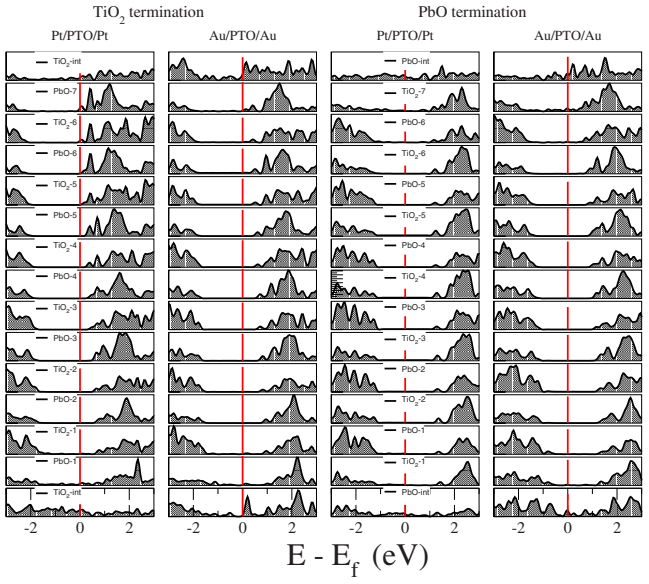

FIG. 2. (Color online) The oxide layer-projected density of states for the TiO_2- and PbO-terminated FE nanocapacitors with Pt and Au electrodes. The polarization is directed upward, i.e., the lower TiO_2 interfacial layer is at the negative surface of the capacitor and the upper one is at the positive surface. All the nanocapacitors have 15 oxide layers (seven unit cells).

From the charge analysis, we conclude the following: (1) there is more charge transfer between the Pt layers and the oxides compared to that between the Au layers and the oxide. This is true in all of the electrodes whether PE or FE, and independent of the termination. This can be understood from the bond strength difference between these metals and oxygen. (2) In the FE case, the electrode layers at the negative surface gain more electron charge than those at the positive surface. In this case, the bond length between the oxygen and the metals is shorter, allowing for more charge transfer and more hybridization between the metal and oxide orbitals. (3) The electrodes at the negative and positive surfaces of the FE nanocapacitor have different chemical environments, i.e., they are not symmetric with respect to the PE phase. (4) In the FE case, charge passivation by the electrodes can be seen, and the amount of passivation can explain the trend that is seen in the nanocapacitor average polarization shown in Table III. For the TiO_2-terminated nanocapacitors, those with the Au electrodes have a larger polarization and also allow for more charge passivation than those with Pt electrodes. With the PbO termination, we see the opposite trend in the passivation of charges and also in the magnitude of the average polarization.

The Löwdin charge analysis helps to explain the behavior seen in the LPDOS. Figure 2 shows LPDOS for the TiO_2- and PbO-terminated FE nanocapacitors with Pt and Au electrodes. In these films, the polarization is directed upward, i.e., the lower interfacial layer is at the negative surface and the upper one is at the positive surface.

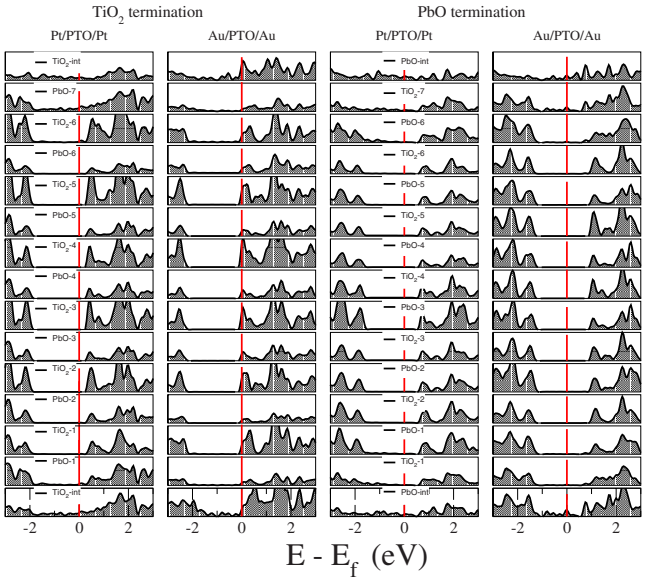

FIG. 3. (Color online) Same as Fig. 2 but for the paraelectric nanocapacitors.

Examining the LPDOS we make the following general comments relevant to all of the nanocapacitors. First, the interfacial oxide layers are metallic with large density of states at the Fermi level. As explained before from the Löwdin charge analysis, there is a considerable amount of charge transfer taking place at the interface. Also, we note that the LPDOS of the PE film in Fig. 3 also shows a metallic behavior of the interfacial layers, in agreement with the charge-transfer picture obtained from the Löwdin orbital analysis. Second, due to the polarization, the valence band at the negative surface is shifted upward, and the conduction band at the positive surface is shifted downward. Third, far from the interface, we can see that the LPDOS of all of the oxide layers are similar to those of bulk PTO.

IV. SUMMARY

We used the recently introduced GGA-PBEsol functional in a study of ferroelectricity in bulk and thin films. GGA-PBEsol seems to yield an accurate description of bulk PTO which is very comparable to that obtained using the GGA-WC functional, and superior to those obtained with GGA-PBE and LDA functionals. In the PTO nanocapacitors with Pt and Au electrodes, we found a critical thickness around 6–7 unit cells ≈24–28 Å. In our study, we constrained the in-plane lattice constant to 3.905 Å, which is the experimental lattice constant of STO. We found that the FE properties of the nanocapacitors depend not only on the electrode type but also on the oxide-electrode termination, even for the same electrode material. This was seen, for example, in the average polarization of the FE film. With Pt electrodes and TiO_2 termination, the film retains 62% of the bulk polarization while with PbO termination, it retains a larger amount (95%) of the bulk polarization. With Au electrodes, we see the opposite behavior, where the film has 80% of the bulk polarization with TiO_2 termination, and a smaller amount (35%) with the PbO termination. These results can be understood in terms of charge passivation, as verified by a Löwdin charge decomposition. The charge analysis shows that the nanocapacitors with Au electrodes and TiO_2 termination passivate the charges better than those with Pt electrodes. On the other hand, for PbO termination, our charge analysis shows that the Pt electrodes passivate the charges more efficiently than those with the Au electrodes.

ACKNOWLEDGMENTS

We would like to thank Ilya Grinberg for reading the manuscript. A.M.R. was supported by the Air Force Office of Scientific Research, Air Force Materiel Command, USAF, under Grant No. FA9550-10-1-0248. W.A.S. was supported by the Department of Energy, Office of Basic Energy Sciences, under Grant No. DE-FG02-07ER15920. Both authors acknowledge computational support from the High-Performance Computing Modernization Office of the Department of Defense.

[1] P. R. Evans, X. Zhu, P. Baxter, M. McMillen, J. McPhillips, F. D. Morrison, J. F. Scott, R. J. Pollard, R. M. Bowman, and J. M. Gregg, Nano Lett. **7**, 1134 (2007).
[2] W. Lee, H. Han, A. Lotnyk, M. A. Schubert, S. Senz, M. Alexe, D. Hesse, S. Baik, and U. Gosele, Nat. Nanotechnol. **3**, 402 (2008).
[3] R. R. Mehta, B. D. Silverman, and J. T. Jacobs, J. Appl. Phys. **44**, 3379 (1973).
[4] J. Junquera and P. Ghosez, Nature (London) **422**, 506 (2003).
[5] C.-G. Duan, R. F. Sabirianov, W.-N. Mei, S. S. Jaswal, and E. Y. Tsymbal, Nano Lett. **6**, 483 (2006).
[6] N. Sai, A. M. Kolpak, and A. M. Rappe, Phys. Rev. B **74**, 059901(E) (2006).
[7] Y. Umeno, B. Meyer, C. Elsässer, and P. Gumbsch, Phys. Rev. B **74**, 060101(R) (2006).
[8] A. M. Kolpak, N. Sai, and A. M. Rappe, Phys. Rev. B **74**, 054112 (2006).
[9] J. E. Spanier, A. M. Kolpak, J. J. Urban, I. Grinberg, L. Ouyang, W. S. Yun, A. M. Rappe, and H. Park, Nano Lett. **6**, 735 (2006).
[10] G. Gerra, A. K. Tagantsev, N. Setter, and K. Parlinski, Phys. Rev. Lett. **96**, 107603 (2006).
[11] G. Gerra, A. K. Tagantsev, and N. Setter, Phys. Rev. Lett. **98**, 207601 (2007).
[12] J. Junquera and P. Ghosez, J. Comput. Theor. Nanosci. **5**, 2071 (2008).
[13] M. Stengel, D. Vanderbilt, and N. A. Spaldin, Nature Mater. **8**, 392 (2009).
[14] J. P. Perdew, A. Ruzsinszky, G. I. Csonka, O. A. Vydrov, G. E.

Scuseria, L. A. Constantin, X. Zhou, and K. Burke, Phys. Rev. Lett. **100**, 136406 (2008).
[15] J. P. Perdew and Y. Wang, Phys. Rev. B **45**, 13244 (1992).
[16] J. P. Perdew, K. Burke, and M. Ernzerhof, Phys. Rev. Lett. **77**, 3865 (1996).
[17] Z. Wu and R. E. Cohen, Phys. Rev. B **73**, 235116 (2006).
[18] M. Stengel and N. A. Spaldin, Nature (London) **443**, 679 (2006).
[19] X. Gonze, J.-M. Beuken, R. Caracas, F. Detraux, M. Fuchs, G.-M. Rignanese, L. Sindic, M. Verstraete, G. Zerah, F. Jollet, M. Torrent, A. Roy, M. Mikami, P. Ghosez, J.-Y. Raty, and D. Allan, Comput. Mater. Sci. **25**, 478 (2002).
[20] http://www.quantum-espresso.org
[21] A. M. Rappe, K. M. Rabe, E. Kaxiras, and J. D. Joannopoulos, Phys. Rev. B **41**, 1227 (1990).
[22] http://opium.sourceforge.net
[23] D. C. Allan and M. P. Teter, J. Am. Ceram. Soc. **73**, 3247 (1990).
[24] H. J. Monkhorst and J. D. Pack, Phys. Rev. B **13**, 5188 (1976).
[25] A. D. Polli, T. Wagner, T. Gemming, and M. Rühle, Surf. Sci. **448**, 279 (2000).
[26] S. A. Mabud and A. M. Glazer, J. Appl. Crystallogr. **12**, 49 (1979).
[27] G. Shirane, H. Danner, and R. Pepinsky, Phys. Rev. **105**, 856 (1957).
[28] V. Milman, B. Winkler, J. A. White, C. J. Pickard, M. C. Payne, E. V. Akhmatskaya, and R. H. Nobes, Int. J. Quantum Chem. **77**, 895 (2000).
[29] M. E. Lines and A. M. Glass, *Principles and Applications of Ferroelectrics and Related Materials* (Clarendon Press, Oxford, 1977).
[30] H. H. Wieder, Phys. Rev. **99**, 1161 (1955).
[31] R. D. King-Smith and D. Vanderbilt, Phys. Rev. B **49**, 5828 (1994).
[32] D. I. Bilc, R. Orlando, R. Shaltaf, G.-M. Rignanese, J. Iniguez, and P. Ghosez, Phys. Rev. B **77**, 165107 (2008).
[33] A. Baldereschi, S. Baroni, and R. Resta, Phys. Rev. Lett. **61**, 734 (1988).
[34] A. Szabo and N. Ostlund, *Modern Quantum Chemistry* (Dover, New York, 1996).